Transcription repressor Bach2 is required for pulmonary surfactant homeostasis and alveolar macrophage function

Atsushi Nakamura,[1,2] Risa Ebina-Shibuya,[1,2] Ari Itoh-Nakadai,[1,4] Akihiko Muto,[1,4] Hiroki Shima,[1,4] Daisuke Saigusa,[5] Junken Aoki,[6] Masahito Ebina,[2] Toshihiro Nukiwa,[2] and Kazuhiko Igarashi[1,3,4]

[1]Department of Biochemistry, [2]Division of Respiratory Medicine, and [3]Center for Regulatory Epigenome and Diseases, Tohoku University Graduate School of Medicine, Sendai 980-8575, Japan
[4]CREST, Japan Science and Technology Agency, Sendai 980-8575, Japan
[5]Department of Integrative Genomics, Tohoku Medical Megabank, Tohoku University, Sendai 980-8573, Japan
[6]Department of Molecular and Cellular Biochemistry, Graduate School of Pharmaceutical Sciences, Tohoku University, Sendai 980-8578, Japan

Pulmonary alveolar proteinosis (PAP) results from a dysfunction of alveolar macrophages (AMs), chiefly due to disruptions in the signaling of granulocyte macrophage colony–stimulating factor (GM-CSF). We found that mice deficient for the B lymphoid transcription repressor BTB and CNC homology 2 (Bach2) developed PAP-like accumulation of surfactant proteins in the lungs. Bach2 was expressed in AMs, and *Bach2*-deficient AMs showed alterations in lipid handling in comparison with wild-type (WT) cells. Although *Bach2*-deficient AMs showed a normal expression of the genes involved in the GM-CSF signaling, they showed an altered expression of the genes involved in chemotaxis, lipid metabolism, and alternative M2 macrophage activation with increased expression of Ym1 and arginase-1, and the M2 regulator Irf4. Peritoneal *Bach2*-deficient macrophages showed increased Ym1 expression when stimulated with interleukin-4. More eosinophils were present in the lung and peritoneal cavity of *Bach2*-deficient mice compared with WT mice. The PAP-like lesions in *Bach2*-deficient mice were relieved by WT bone marrow transplantation even after their development, confirming the hematopoietic origin of the lesions. These results indicate that Bach2 is required for the functional maturation of AMs and pulmonary homeostasis, independently of the GM-CSF signaling.

CORRESPONDENCE
Kazuhiko Igarashi:
igarashi@med.tohoku.ac.jp

Abbreviations used: AM, alveolar macrophage; Bach2, BTB and CNC homology 2; BAL, bronchoalveolar lavage; BMDM, BM-derived macrophage; GO, gene ontology; LC-MS/MS, liquid chromatography–mass spectrometry; Lxrα, liver X receptor α; PAP, pulmonary alveolar proteinosis; PAS, periodic acid-Schiff; PC, phosphatidylcholine; Pparγ, peroxisome proliferator-activated receptor γ; SP, surfactant protein.

The normal function of the lung, including gas exchange, requires the production of pulmonary surfactant. Pulmonary alveolar proteinosis (PAP) is a rare fatal syndrome accompanied by an abnormal accumulation of pulmonary surfactant in the alveolar spaces of the lungs (Trapnell et al., 2003; Borie et al., 2011). Pulmonary surfactant is composed mainly of phospholipids, neutral lipids (mainly of cholesterol), and four kinds of protein, known as surfactant protein (SP)-A (encoded by *Sftpa1*), SP-B (*Sftpb*), SP-C (*Sftpc*), and SP-D (*Sftpd*). Surfactant makes up the air-liquid interface of the alveolar wall to prevent alveolar collapse. It also contributes to pulmonary host defense by opsonization of microbial pathogens. Surfactant homeostasis is regulated by two types of cells. Surfactant is produced and secreted by the alveolar type 2 epithelial cells, and is taken up by them and reused. In addition, excess surfactant is phagocytized by alveolar macrophages (AMs), the resident mononuclear phagocytes in the respiratory tract, and is catabolized (Trapnell et al., 2003).

Clinically, PAP is classified into three types: acquired, congenital, and secondary. Several observations have suggested that dysfunctions of AMs are causative to PAP. Acquired PAP is a result of neutralizing autoantibodies against

A. Nakamura and R.E. Shibuya contributed equally to this paper.
M. Ebina's present address is Pulmonary Center, Tohoku Pharmaceutical University Hospital, 1-12-1 Fukumuro, Sendai 983-8512, Japan.

The Rockefeller University Press $30.00
J. Exp. Med. 2013 Vol. 210 No. 11 2191-2204
www.jem.org/cgi/doi/10.1084/jem.20130028

The Journal of Experimental Medicine

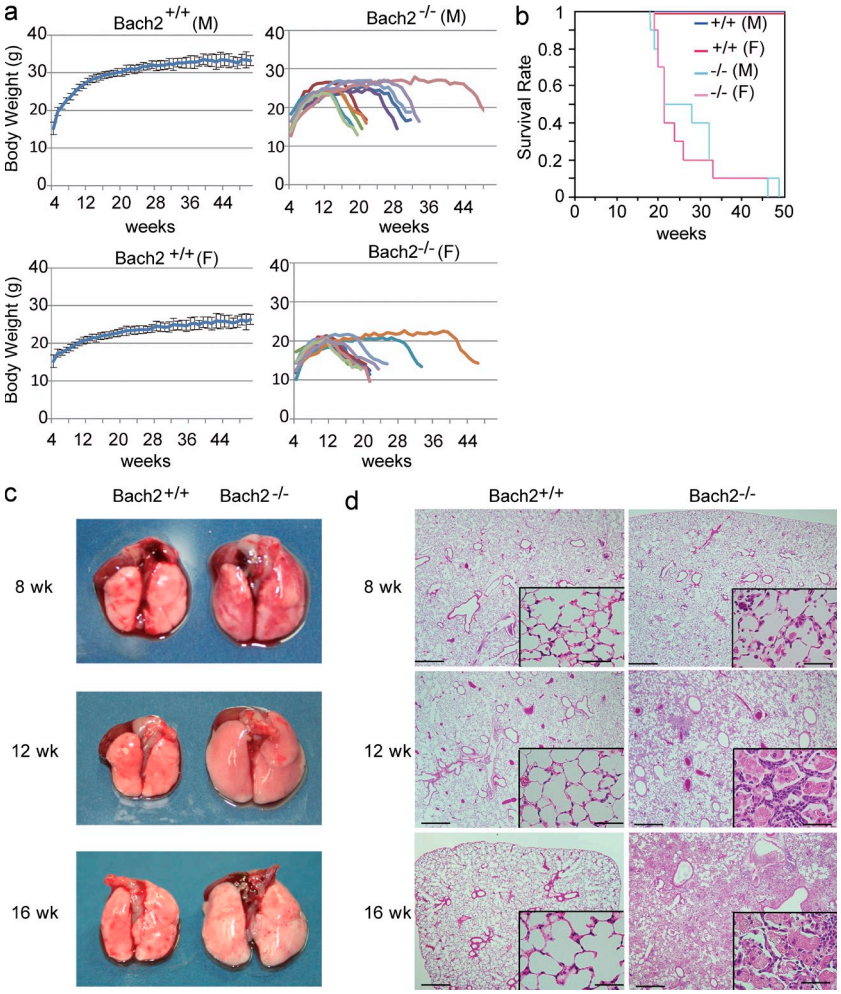

Figure 1. PAP-like disease in *Bach2*-deficient mice. (a) The body weight curves of WT and *Bach2*-deficient male and female mice (n = 10/group). The data from the WT mice are shown as the mean with the SD, whereas the data from *Bach2*-deficient mice are shown individually because *Bach2*-deficient mice showed individual variability in body weight and longevity. (b) The survival curves of WT and *Bach2*-deficient mice. WT male (M) and female (F) mice were combined. The curves for *Bach2*-deficient male (light blue, n = 10) and female (pink, n = 10) mice are shown separately. (c) The macroscopic appearance of the lungs of WT and *Bach2*-deficient mice at indicated time points. (d) HE staining of paraffin-embedded lungs from the WT and *Bach2*-deficient mice. Bars: 500 µm; (insets) 50 µm.

GM-CSF (Kitamura et al., 1999; Inoue et al., 2008), indicating that GM-CSF signaling is essential for AM maturation and function. Congenital PAP is associated with mutations in genes encoding the GM-CSF receptor βc chain (*Csf2rb*; Dirksen et al., 1997), SP-B (Nogee et al., 1993), or SP-C (Nogee et al., 2001). Secondary PAP, which is the most common form of PAP, accompanies other diseases such as hematological cancers (Buechner and Ansari, 1969; Ruben and Talamo, 1986; Cordonnier et al., 1994; Keller et al., 1995; Ladeb et al., 1996; Trapnell et al., 2003). Although secondary PAP may also involve a dysfunction of AMs, its etiology is unclear. As a result, patients with secondary PAP are difficult to cure, thereby necessitating further elucidation of the functions and regulation of AMs.

Macrophages play diverse functions such as innate immunity, inflammation, tissue repair, and iron homeostasis depending on their location and the stimuli they receive (Mosser and Edwards, 2008). Macrophages show functionally polarized phenotypes in a signal- and context-dependent manner. In response to cytokines such as interferon-γ and bacterial components like LPS, macrophages become polarized to show the classical activated M1 phenotype with increased microbicidal activity mediating the initial inflammatory response (Gordon, 2003; Mosser and Edwards, 2008; Martinez, 2011). In response to Th2 cytokines Il-4 and Il-13, they become polarized to show the alternative M2 phenotype, which is important for debris scavenging, tissue remodeling, and wound healing after inflammation (Gordon, 2003; Mosser and Edwards, 2008; Martinez, 2011). Although the functional diversity of macrophages has been appreciated for a long while, the mechanisms that regulate the acquisition of particular functional states in terms of gene expression are just emerging. Transcription factors Irf4 and Stat6 promote M2 polarization (Satoh et al., 2010; Lawrence and Natoli, 2011; Nelson et al., 2011), and Spi-C is required for the differentiation of red pulp macrophages of the spleen specialized in iron homeostasis (Kohyama et al., 2009).

BTB and CNC homology 2 (Bach2) has been regarded as a B cell–specific transcription factor which associates with the Maf recognition elements (MAREs) of DNA (Oyake et al., 1996). Its expression is high from pro–B cells to mature B cells, whereas it is low in terminally differentiated plasma cells (Muto et al., 1998). Genetic ablation of *Bach2* results in severe reduction in DNA class switch recombination (CSR) and somatic hypermutation, with a concomitant increase in IgM production (Muto et al., 2004). Bach2 represses the

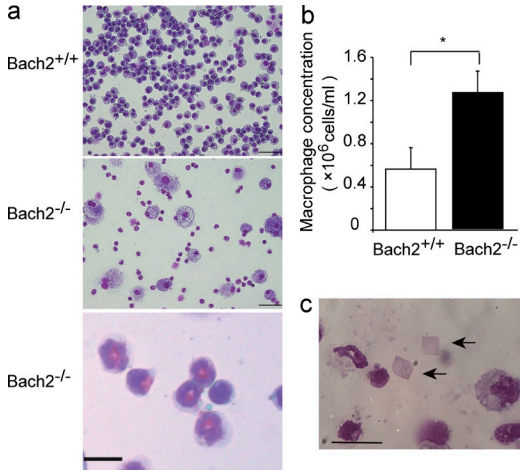

Figure 2. PAP-like disease in *Bach2*-deficient mice. (a) May-Giemsa staining of BAL cells from WT and *Bach2*-deficient mice. Bars, 100 µm. An enlarged panel is at the bottom to show eosinophils (bar, 10 µm). (b) Cell concentrations of AMs in BAL fluids from WT and *Bach2*-deficient mice. The mean values from five mice for each group are shown. Error bars represent SD. P-values were obtained by two-tailed Student's *t*-tests. *, $P < 0.05$. (c) Crystal polygons (arrows) in the BAL fluid from *Bach2*-deficient mice. Bar, 20 µm.

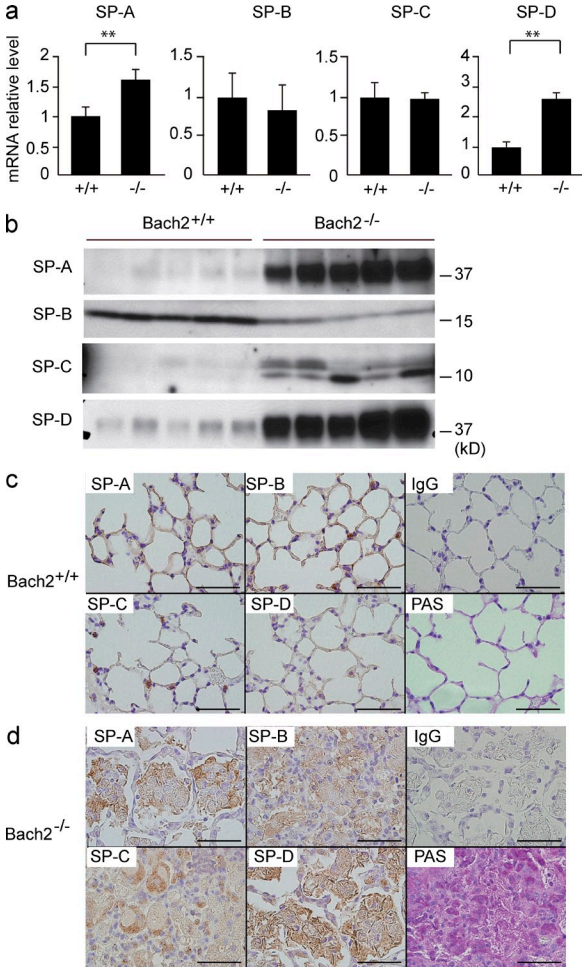

Figure 3. The accumulation of SPs in *Bach2*-deficient lungs. (a) The mRNA levels of *SP-A*, *-B*, *-C*, and *-D* in the lungs were determined by quantitative RT-PCR. mRNA of β-Actin was used as a normalization control. The mean values from five mice for each group are shown. P-values were obtained by two-tailed Student's *t*-tests. Error bars represent SD. **, $P < 0.01$. (b) SPs were compared by Western blot analysis of the BAL fluids from WT and *Bach2*-deficient mice ($n = 5$). (c and d) An immunohistochemical analysis of WT (c) and *Bach2*-deficient (d) lungs using antibodies against SP-A, -B, -C, -D, or control IgG. The results of PAS staining are also shown. Bars, 50 µm.

expression of Blimp-1, the key regulator of plasma cell differentiation, and thereby inhibits plasma cell differentiation (Ochiai et al., 2006; Muto et al., 2010). The Bach2-mediated repression of the Blimp-1 gene is essential for CSR and the expression of its executing molecule AID (Muto et al., 2010). Although Bach2 is also expressed in hematopoietic progenitors (unpublished data), its expression and function in macrophages have not yet been reported. We herein report our discovery that *Bach2*-deficient mice develop PAP-like pulmonary histopathology. Our data were obtained by analyzing AMs and using BM transplantation, and suggest that Bach2 has an important role in tuning the function of AMs with regard to surfactant homeostasis in the lungs. We further show that Bach2 represses the M2 polarization of alveolar and peritoneal macrophages, extending its function to innate immunity.

RESULTS

Bach2-deficient mice develop PAP-like lesions with progressive dyspnea

Bach2-deficient mice were born at the Mendelian ratio and thrived almost as much as WT mice for the first 3 mo. However, they gradually started to show slow movement with progressive dyspnea and body weight loss irrespective of sex (Fig. 1 a), and started to die as early as 18 wk of age (Fig. 1 b). Because *Bach2*-deficient mice became moribund with dyspnea, we examined the alterations in their lungs over time. Although the sizes of the lungs in 8-wk-old *Bach2*-deficient mice were similar to those in WT mice (Fig. 1 c), the alveolar spaces of *Bach2*-deficient mice were infiltrated with large AMs and granulocytes (Fig. 1 d). At 12 wk of age, the lungs of the *Bach2*-deficient mice became obviously larger than those of WT mice (Fig. 1 c). Their alveolar spaces began to be filled with pink materials and inflammatory cells. Proliferation of the alveolar epithelial cells was also apparent (Fig. 1 d). These changes further deteriorated at 16 wk of age (Fig. 1, c and d). The bronchoalveolar lavage (BAL) fluid of *Bach2*-deficient mice showed a milky appearance, thus suggesting the accumulation of pulmonary surfactant (unpublished data). A cytological examination of the BAL cells showed that the majority of the cells were AMs in the WT mice. In contrast, we observed an increased number of AMs which looked foamy in appearance, and more eosinophils and neutrophils were also recruited in the BAL fluid of *Bach2*-deficient mice (Fig. 2, a and b). The presence of eosinophils and neutrophils were confirmed by flow cytometry of BAL cells using F4/80 and Gr-1 antibodies (unpublished data). A similar infiltration

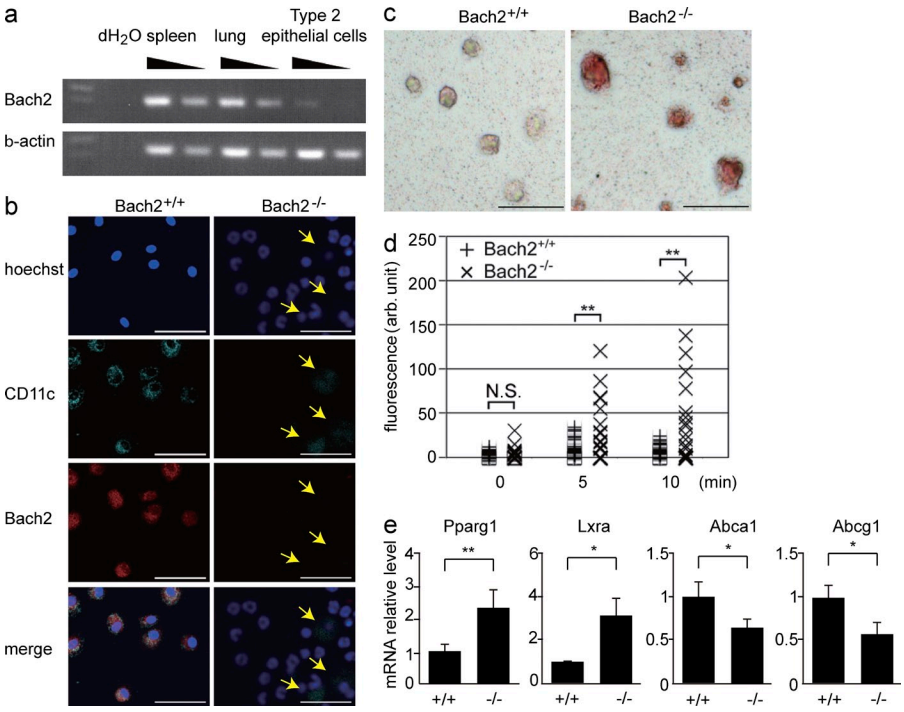

Figure 4. *Bach2*-deficient AMs show defects in phagocytosis and cholesterol handling. (a) The *Bach2* expression in the spleen, lung, and alveolar type 2 epithelial cells was determined by semi-quantitative RT-PCR. β-Actin mRNA was used as a normalization control. (b) The Bach2 expression in BAL cells was examined by immunofluorescence staining. Hoechst (blue), CD11c (green), Bach2 (red), and merged images are shown. The CD11c-positive cells (arrows) were AMs. Bars, 50 µm. (c) Oil-Red O staining of AMs from WT and *Bach2*-deficient AMs. The experiments were performed independently three times (bars, 100 µm). (d) Uptake of cholesterol by indicated AMs was determined and shown as relative fluorescence intensities per cell. P-values were obtained by two-tailed Student's *t*-tests. **, $P < 0.01$; N.S., nonsignificant. (e) The mRNA levels of *Pparγ1*, *Lxrα*, *Abca1*, and *Abcg1* in sorted AMs were determined by quantitative RT-PCR. β-Actin expression was used as a normalization control. The mean values from WT ($n = 3$) and *Bach2*-deficient ($n = 4$) AMs are shown. The error bars represent SD. P-values were obtained by two-tailed Student's *t* tests. **, $P < 0.01$; *, $P < 0.05$.

of granulocytes in the lungs is also found in secondary PAP patients (Ando et al., 2002). We also observed crystal polygon in the BAL fluid (Fig. 2 c) which looked like the Ym1 crystal observed in *SHIP*-deficient mice (Rauh et al., 2005).

We assessed the expression of SPs in the lungs. The mRNA expression levels of SP-A and SP-D were increased in *Bach2*-deficient mice (Fig. 3 a). An immunoblotting analysis of BAL fluids revealed that the amounts of SP-A, SP-C, and SP-D were increased in *Bach2*-deficient mice (Fig. 3 b). In an immunohistochemical analysis of WT mice, SPs were detected in the alveolar type 2 epithelial cells and alveolar walls (Fig. 3 c). In contrast, the accumulated materials in the alveolar spaces of *Bach2*-deficient mice were positive for all SPs (Fig. 3 d). Moreover, the deposits in the alveolar spaces were periodic acid-Schiff (PAS)–positive (Fig. 3 d), indicating that the accumulated pink materials were pulmonary surfactant (Trapnell et al., 2003). Collectively, these findings showed that *Bach2*-deficient mice developed PAP-like disease.

Altered lipid handling of *Bach2*-deficient AMs

Because pulmonary surfactant is secreted by alveolar type 2 epithelial cells and is phagocytized by AMs, we investigated the expression of Bach2 in these cells. The expression of *Bach2* was hardly detected in the isolated alveolar type 2 epithelial cells by the RT-PCR (Fig. 4 a) or immunohistochemical analyses of the lungs using anti-Bach2 antibodies (not depicted). In contrast, we detected Bach2 in WT but not *Bach2*-deficient AMs by immunostaining (Fig. 4 b).

A substantial part of pulmonary surfactant is lipid, including phospholipids and cholesterol, which are taken up by AMs (Trapnell et al., 2003). The foamy AMs associated with PAP are due to their ingestion of a large amount of lipids (Iyonaga et al., 1999). We detected a prominent accumulation of lipids in *Bach2*-deficient AMs by Oil-Red O staining (Fig. 4 c). We also found that *Bach2*-deficient AMs showed an enhancement in cholesterol uptake in vitro compared with WT control cells (Fig. 4 d). Peroxisome proliferator-activated receptor γ (Pparγ) and liver X receptor α (Lxrα) play pivotal roles in the regulation of cholesterol metabolism in macrophages. These transcription factors are activated by oxysterols, oxidized derivatives of cholesterol, and transactivate ATP-binding cassette transporters A1 (*Abca1*) and G1 (*Abcg1*), which excrete excess cholesterol from macrophages (Chawla et al., 2001; Bonfield et al., 2003; Ricote et al., 2004; Bates et al., 2005; Baker et al., 2010). Although the mRNA levels of *Pparg1* and *Lxrα* were increased in *Bach2*-deficient AMs compared with WT cells, the mRNA levels of *Abca1* and *Abcg1* were decreased (Fig. 4 e). These results suggest that the enhanced uptake of cholesterol and the changes in gene expression related to cholesterol efflux in *Bach2*-deficient AMs were connected with the onset of the PAP-like disease.

Phospholipid compositions of AMs were compared using liquid chromatography–mass spectrometry (LC-MS/MS) analysis. We focused on phosphatidylcholines (PCs), including palmitoyl-palmitoleoyl PC (PC16:0/16:1, characterized by the presence of one saturated and one unsaturated fatty acid), PC16:0/18:2, PC16:0/18:1, and other related PC species which are the major surfactant lipids (Postle et al., 2006). The representative mass chromatograms by precursor ion scanning mode are shown in Fig. 5 a. As shown in Fig. 5 b, many of

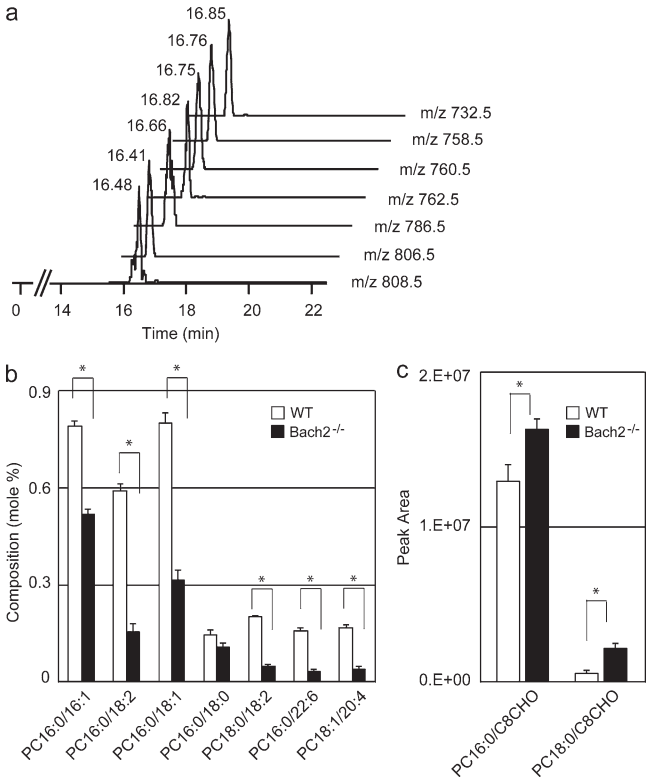

Figure 5. *Bach2*-deficient AMs show alterations in lipid handling. (a) PC16:0/16:1, PC16:0/18:2, PC16:0/18:1, PC16:0/18:2, PC18:0/18:1, PC16:0/22:6, and PC18:1/20:4 were assigned from the value of m/z 732.5, 758.5, 760.5, 762.5, 786.5, 806.5, and 808.5. (b and c) The composition of representative spices of PCs (b) and oxidized PCs (oxPCs; c) were compared between AMs isolated from WT and *Bach2*-deficient mice. OxPCs: PC16:0/C8CHO and PC18:0/C8CHO were assigned from the value of m/z 650.5 and 678.5, respectively. The values of PCs and oxPCs were presented by their peak ratio using TSQ Quantum Ultra and peak area using Q Exactive, respectively, and expressed as mean ± SD. Statistical analysis were performed using a Student's *t* test for comparisons between the two genetic backgrounds, and values of $P < 0.05$ (*) were considered statistically significant.

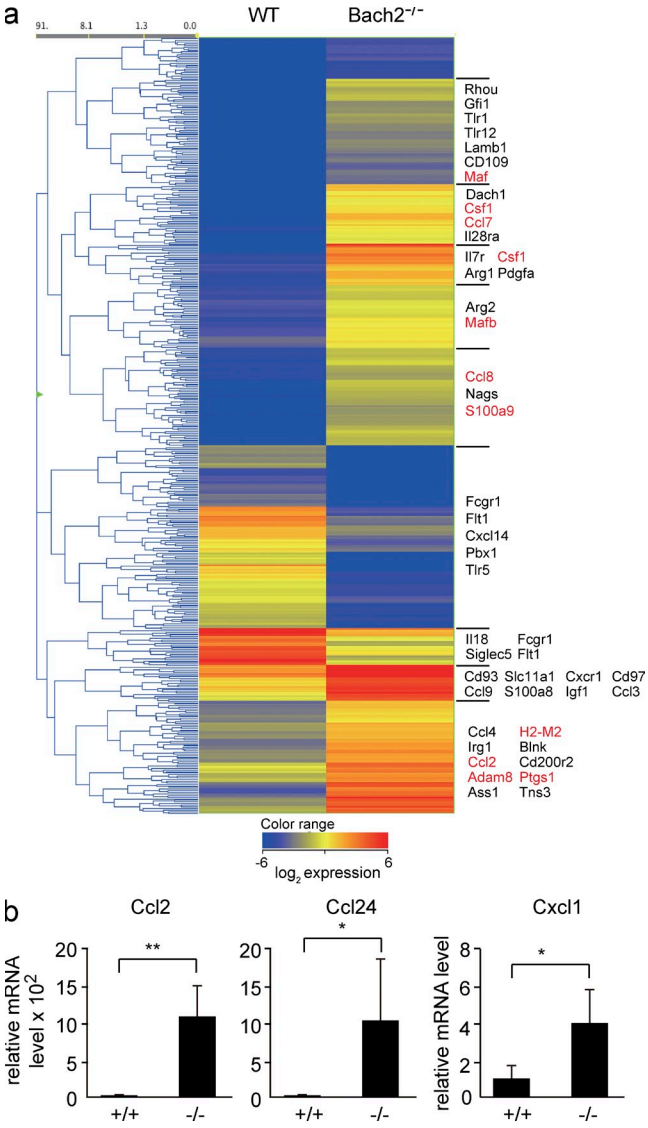

Figure 6. The gene expression profile of *Bach2*-deficient AMs. (a) The heat-map of genes showing >10-fold changes in expression between WT and Bach2$^{-/-}$ AMs. Genes involved in cytokine signaling, chemotaxis, lipid metabolism, arginine metabolism, and gene expression are arbitrarily shown. (b) The mRNA levels of *Ccl2*, *Ccl24*, and *Cxcl1* in sorted AMs were determined by quantitative RT-PCR. β-Actin mRNA was used as the normalization control. The mean values were shown from WT ($n = 3$) and *Bach2*-deficient ($n = 4$) AMs. The error bars represent SD. The p-values were obtained by two-tailed (Ccl2 and Cxcl1) or one-tailed (Ccl24) Student's *t* tests. **, $P < 0.01$; *, $P < 0.05$.

these PC species were reduced in *Bach2*-deficient AMs compared with WT AMs. We identified two oxidized forms of PCs which were increased in *Bach2*-deficient AMs (Fig. 5 c). These altered levels of PCs and oxidized PCs point to a defective handling of the surfactant lipids by *Bach2*-deficient AMs.

The GM-CSF–PU.1 pathway is not impaired in *Bach2*-deficient mice

GM-CSF stimulation is essential for the functional maturation of AMs. GM-CSF binds to the GM-CSF receptor to induce PU.1 expression, which then drives the terminal differentiation of AMs (Shibata et al., 2001; Trapnell et al., 2009). A segment of PAP patients (Dirksen et al., 1997; Kitamura et al., 1999) and *GM-CSF*–deficient mice (Dranoff et al., 1994) show a disruption of the GM-CSF signaling in AMs, thus resulting in impaired phagocytosis (Harris, 1979; Paine et al., 2001; Yoshida et al., 2001) and cholesterol efflux (Thomassen et al., 2007; Blanchard et al., 2012), which contribute to the foamy AMs found in PAP. We therefore looked for an alteration in the GM-CSF pathway in *Bach2*-deficient mice. The mRNA levels of GM-CSF in the lungs and the concentrations of GM-CSF in the BAL fluids were not decreased in the *Bach2*-deficient mice (unpublished data). Furthermore, the mRNA levels of GM-CSF receptor subunits α and β (GM-CSFRα and GM-CSFRβc) and PU.1 in sorted AMs were not decreased by *Bach2* deficiency (unpublished data). Immunostaining of BAL cells verified that PU.1 was expressed

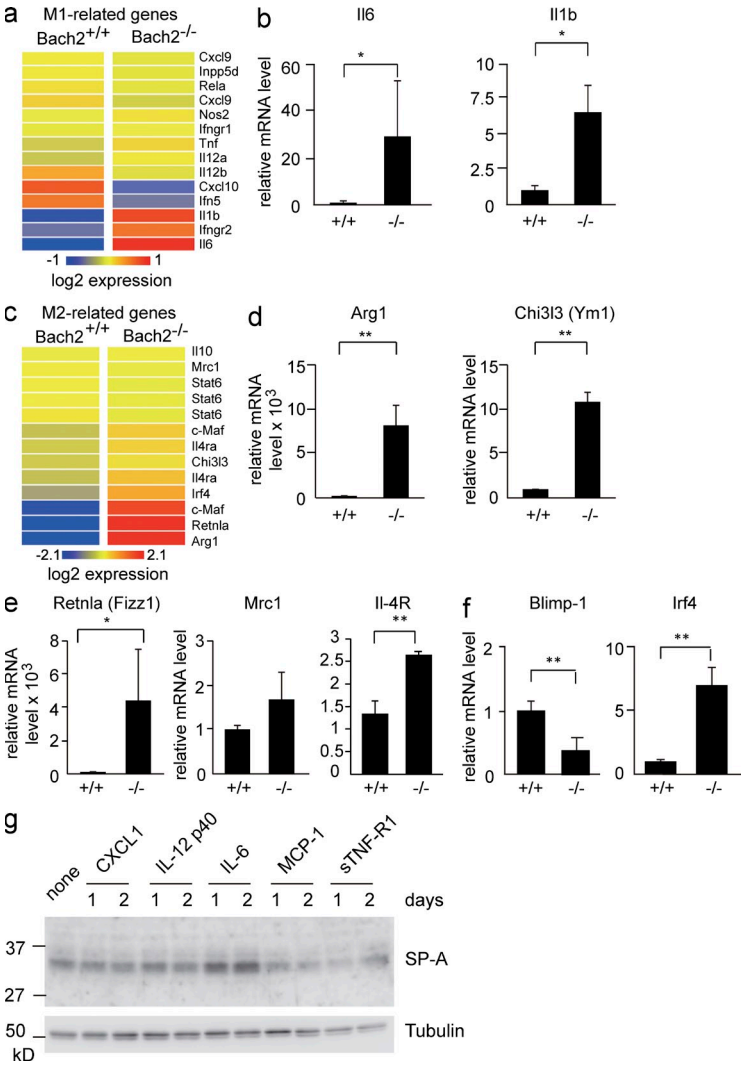

Figure 7. Expression of M1- and M2-related genes in *Bach2*-deficient AMs. (a) The heat-map of M1-related genes. (b) The mRNA levels of *Il-6* and *Il-1b* in sorted AMs were determined by quantitative RT-PCR. (c) The heat-map of M2-related genes. (d and e) The mRNA levels of *Arg1*, *Ym1*, *Fizz1*, *Mrc1*, and *IL-4R* in sorted AMs were determined by quantitative RT-PCR. (f) The mRNA levels of *Blimp-1* and *Irf4* in sorted AMs were determined by quantitative RT-PCR. (b and d–f) β-Actin mRNA was used as the normalization control. The mean values were shown from WT ($n = 3$) and *Bach2*-deficient ($n = 4$) AMs. The error bars represent SD. The p-values were obtained by two-tailed Student's *t* tests, except Il6 and Retnla (one-tailed tests). *, $P < 0.05$; **, $P < 0.01$. (g) H441 lung adenocarcinoma cells were treated with the indicated reagents for 1 or 2 d, and the levels of SP-A protein were determined by Western blot analysis. A representative result of two independent experiments is shown.

normally in *Bach2*-deficient AMs (unpublished data). Therefore, the expression of the central components of the GM-CSF pathway was not affected by the *Bach2* deficiency.

In humans, PAP frequently involves anti–GM-CSF autoantibodies (Kitamura et al., 1999). Therefore, we investigated whether anti–GM-CSF antibodies were involved in the pathogenesis of PAP in the *Bach2*-deficient mice because they tend to produce autoantibodies (unpublished data). Blimp-1 (*Prdm1*) is the master regulator of plasma cells, and *Blimp-1*–deficient mice cannot secret any antibodies (Shapiro-Shelef et al., 2003). We crossbred *Bach2*-deficient mice and B cell–specific *Blimp-1*–deficient mice (Shapiro-Shelef et al., 2003) and obtained *Bach2*-deficient mice which could not secret any antibodies. Although the *Blimp-1*–deficient mice did not develop PAP, the *Bach2* and *Blimp-1* double-deficient mice developed PAP as severely as did the *Bach2*-deficient mice (unpublished data). These results showed that autoantibodies were not involved in the pathogenesis of PAP in *Bach2*-deficient mice. Collectively, these data suggested that the dysfunction of *Bach2*-deficient AMs was independent of the GM-CSF-PU.1 pathway.

Altered expression of genes for immune cell trafficking in macrophages

To reveal the genes downstream of Bach2 in AMs, we compared the gene expression profiles of AMs using a microarray analysis. We focused on genes whose expression changed >10-fold in the absence of Bach2 (Fig. 6 a). Consistent with the increased infiltration of AMs and granulocytes in *Bach2*-deficient mice (Fig. 2), gene ontology (GO) analysis of these genes revealed that GO categories related to inflammatory response and immune cell trafficking tended to be enriched in *Bach2*-deficient AMs (Table S2). These categories included genes such as *Ccl2*, *Ccl7*, *Ccl8*, *Csf1*, *S100a9*, *Adam8*, and *MafB* (Fig. 6 a). The altered lipid handling of *Bach2*-deficient macrophages was also supported by the enrichment of GO terms related to lipid binding (e.g., *Ptgs1*). The higher expression of *Ccl2*, which encodes monocyte migration cytokine (MCP-1) in *Bach2*-deficient AMs than control AMs, was confirmed using an RT-PCR analysis (Fig. 6 b). *Ccl24* encoding an eosinophil migration cytokine (eotaxin-2) and *Cxcl1* encoding a neutrophil migration chemokine (KC) also

tended to be up-regulated in *Bach2*-deficient AMs in the array analysis (unpublished data) and RT-PCR analysis (Fig. 6 b). Increased levels of Ccl2/MCP-1 and Cxcl1/KC were confirmed by a cytokine antibody array analysis of the BAL fluid (unpublished data). These results suggest that the enhanced recruitment of AMs and granulocytes in the lung of *Bach2*-deficient mice was due, at least in part, to the changes in the expression of genes related to immune cell trafficking in AMs. By focusing on genes whose expression was reduced more than fourfold, *Bach2* deficiency was found to affect MHC class II components (Table S3). Interestingly, expression of MHC class I components such as H2-M2 were increased (Fig. 6 a and not depicted). These observations together suggest that the lung pathology we observed may involve deregulation of the immune system at multiple points.

Aberrant activation of M2-related genes and Irf4 in *Bach2*-deficient AMs

The expression of M1- and M2-related genes was also altered. Among the M1-related genes, although *Nos2* encoding iNOS was not affected, a fraction of the genes showed either decreased (*Cxcl10* and *Ifn5*) or increased (*Il-6* and *Il-1b*) expression (Fig. 7, a and b). Higher levels of Il-6, Il-12, and soluble TNFR1 (sTNFR1) were also present in the BAL fluids from *Bach2*-deficient mice (unpublished data). Many of the M2-related genes were up-regulated in the *Bach2*-deficient AMs, including *Arg1* encoding arginase and *Ym1* encoding chitinase-3–like 3 (Fig. 7, c and d). The expression of two other M2-related genes, *Retnla* and *Mrc1*, also tended to be higher. IL-4 receptor α mRNA was also higher in *Bach2*-deficient AMs than WT cells, raising the possibility of increased IL-4 signaling in *Bach2*-deficient AMs (Fig. 7 e). These results suggested that *Bach2*-deficient AMs showed aberrant activation of M1 and M2 phenotypes.

Irf4 is a critical regulator of M2 polarization (Satoh et al., 2010). We found that the expression of Irf4 was elevated in *Bach2*-deficient AMs (Fig. 7 f). Bach2 represses the expression of Blimp-1, which in turn activates Irf4 in B lymphoid cells (Sciammas et al., 2006; Igarashi et al., 2007; Muto et al., 2010). However, the expression of Blimp-1 was not elevated in *Bach2*-deficient AMs (Fig. 7 f). These results suggest that Bach2 represses Irf4 in a Blimp-1–independent manner in AMs and that the overexpression of Irf4 might contribute to the activation of the M2 phenotype in *Bach2*-deficient AMs.

Based on the above results, we surmised that the altered gene expression in *Bach2*-deficient AMs would affect the production of surfactants in the alveolar cells. To address this possibility, we focused our analysis on Cxcl1, Il-12 p40/IL-12b, Il-6, Ccl2/MCP-1, and sTNF-R1, which showed higher expression in *Bach2*-deficient macrophages than in control WT cells (Figs. 6 and 7) and/or was present at higher levels in BALs of *Bach2*-deficient mice than those of WT mice (not depicted). We used human NCI-H441 cell line which exhibits the characteristics of alveolar type II epithelial cells. As shown in Fig. 7 g, Il-6 enhanced SP-A expression, whereas other factors did not show such an effect. Therefore,

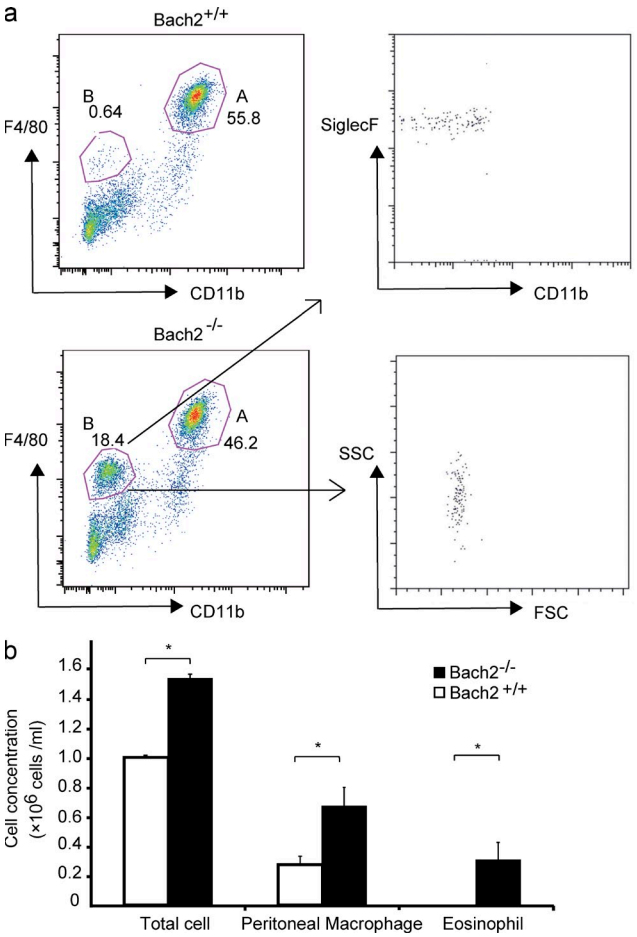

Figure 8. *Bach2*-deficient mice contained more macrophages and eosinophils in peritoneal cavity. (a) The flow cytometric analysis of peritoneal cells isolated from indicated mice. Gates A and B contained macrophages and eosinophils, respectively. (b) The concentrations of total cells, macrophages, and eosinophils in the peritoneal cavity of indicated mice. Results were obtained using three mice per genotypes. The p-values were obtained by two-tailed Student's *t* tests. The error bars represent SD. *, $P < 0.05$.

the altered expression of Il-6 in *Bach2*-deficient AMs may be responsible, at least in part, for the enhanced production of SP-A (Fig. 3 a).

Aberrant activation of M2 phenotype in *Bach2*-deficient peritoneal macrophages

To investigate whether the effect of *Bach2* deficiency upon the macrophage phenotype is restricted to AMs or not, we compared peritoneal macrophages in WT control and *Bach2*-deficient mice. *Bach2*-deficient mice tended to contain higher numbers of peritoneal cells and resident macrophages (Fig. 8, a and b). As was the case in the lung, more F4/80^{low} CD11b^{-} SiglecF^{+} eosinophils were present in the peritoneal cavity of *Bach2*-deficient mice than WT mice (Fig. 8, a and b), suggesting that Bach2 regulated the recruitment of eosinophils. Isolated peritoneal macrophages were stimulated with GM-CSF in vitro in the presence of the M1 inducer LPS or the M2

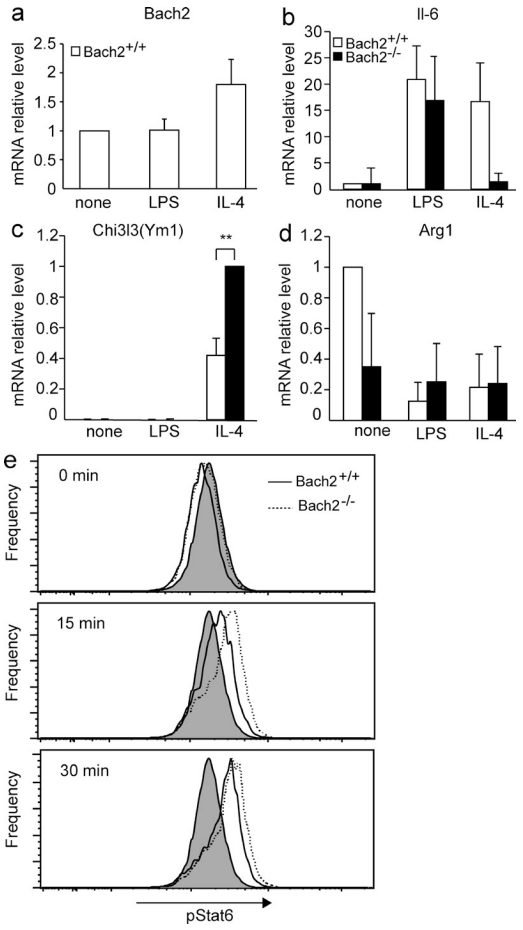

Figure 9. Expression of M1- and M2-related genes in *Bach2*-deficient peritoneal macrophages. Peritoneal macrophages were stimulated with indicated reagents for 48 h in vitro. The mRNA levels of *Bach2* (a), *IL-6* (b), *Ym1* (c), and *Arg1* (d) in the macrophages isolated from indicated mice were determined by quantitative RT-PCR. β-Actin mRNA was used as the normalization control. The mean values were shown ($n = 4$). The error bars represent SD. The p-values were obtained by two-tailed Student's *t* tests. **, $P < 0.01$. (e) Intracellular staining of indicated BMDMs was performed using phosphorylated STAT6 antibody after the stimulation with IL-4 for indicated periods. Signal intensities were analyzed using flow cytometer and shown. Staining with control isotype antibody is shown as gray plots. Representative results of two independent experiments are shown.

inducer IL-4, and their gene expression was compared. Bach2 expression itself in WT cells was not affected by LPS but increased by IL-4 (Fig. 9 a). The expression of IL-6 was strongly induced by either LPS or IL-4 in WT macrophages (Fig. 9 b). Its induction appeared less prominent in the absence of Bach2, although it was not statistically significant (Fig. 9 b). In contrast, M2-related Chi3l3 (Ym1) was more highly expressed in *Bach2*-deficient macrophages than in WT cells in response to IL-4 (Fig. 9 c). The expression of other M2-related genes, including Arg1 and Fizz1, did not differ irrespective of the genotype (Fig. 9 d and not depicted). These results suggest that Bach2 limits a part of M2-like polarization not only in AMs but also in peritoneal macrophages.

Because one of the critical downstream effectors of Il-4 in macrophages is STAT6 (Takeda et al., 1996; Kang et al., 2008; Lawrence and Natoli, 2011), we compared phosphorylation of STAT6 in BM-derived macrophages (BMDMs) isolated from *Bach2*-deficient and control WT mice. We found an enhancement in STAT6 phosphorylation in response to Il-4 in *Bach2*-deficient BMDM as compared with WT cells (Fig. 9 e). Therefore, the enhanced response to Il-4 may contribute the altered phenotypes of *Bach2*-deficient macrophages. The higher expression of Il-4 receptor mRNA (Fig. 7 e) may be causative to this enhanced STAT6 phosphorylation.

The expression of *Bach2* in hematopoietic cells is essential for pulmonary homeostasis

To confirm the involvement of altered hematopoietic cells in the development of PAP-like disease in the *Bach2*-deficient mice, we performed BM transplantation using *Bach2*-deficient mice ($CD45.2^+$) and WT mice ($CD45.1^+CD45.2^+$). First, to examine whether WT BM could prevent the onset of PAP in *Bach2*-deficient mice, we transplanted WT and *Bach2*-deficient BM into 8-wk-old *Bach2*-deficient mice (Fig. 10 a), which we had shown to be at preclinical stage (i.e., less accumulation of surfactant in the alveolar spaces; Fig. 2 a). At 2 mo after transplantation, a flow cytometric analysis of the peripheral blood cells showed efficient replacement by WT cells in *Bach2*-deficient mice transplanted with WT BM (Fig. 10 b). The *Bach2*-deficient mice transplanted with WT BM looked free from dyspnea. Pink materials did not accumulate in the alveolar spaces, and inflammatory cells were not recruited in these mice (Fig. 10 c). In contrast, the *Bach2*-deficient mice transplanted with *Bach2*-deficient BM showed progressive dyspnea and developed PAP as severely as nontreated *Bach2*-deficient mice (Fig. 10, b and c). Therefore, the PAP-like disease with the infiltration of inflammatory cells was caused by *Bach2* deficiency in hematopoietic cells.

Next, to examine whether BM transplantation could ameliorate the PAP-like disease of *Bach2*-deficient mice, we transplanted WT BM into *Bach2*-deficient mice >16 wk of age (Fig. 10 d), which we expected to have already accumulated large amounts of surfactant in the alveolar spaces (Fig. 1). This expectation was confirmed by the CT imaging of these mice before transplantation (Fig. 10 f). Indeed, these *Bach2*-deficient mice had already shown progressive dyspnea. At 2 mo after transplantation, the flow cytometric analysis of peripheral blood cells showed that a part of the BM had been replaced by WT cells (Fig. 10 e). This was because we applied only 500 rads upon the transplantation due to their disease condition (Fig. 10, figure legend). The mice started to show calm and normal breathing after the WT BM transplantation. Before BM transplantation, we observed the diffuse distribution of reticular shadows and partial consolidation shadows in the CT images of the lungs of these mice (Fig. 10 f). After transplantation, these findings dramatically improved, and the diffuse reticular shadows became lighter and the consolidation shadows almost disappeared (Fig. 10 f). Although foamy AMs and granulocytes still existed in the alveolar

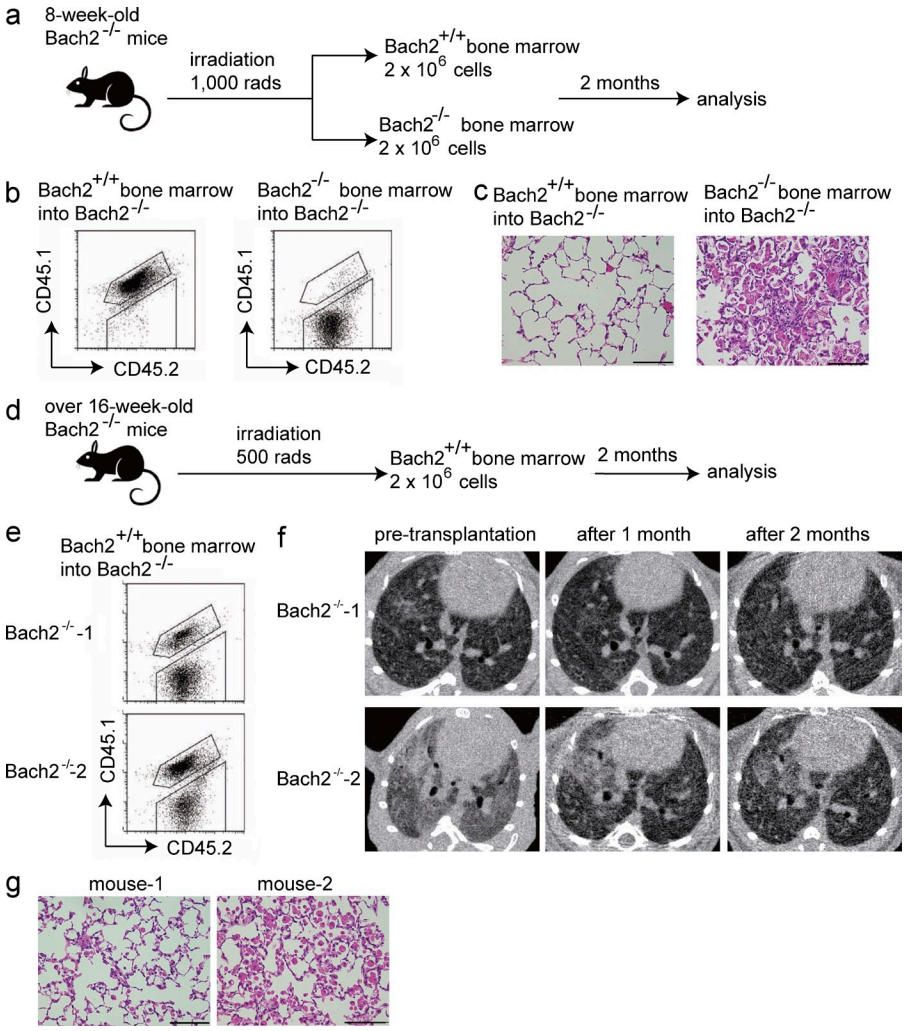

Figure 10. The expression of *Bach2* in hematopoietic cells is essential for pulmonary homeostasis. (a) The protocol for the BM transplantation to examine the effects on PAP. The experiments were performed using three mice for each group. (b) The flow cytometric analysis of peripheral blood cells to confirm the success of the transplant. (c) The histological examination (HE staining) of the lungs 2 mo after BM transplantation. Bars, 100 µm. (d) The protocol for the BM transplantation to examine the therapeutic effects. Because *Bach2*-deficient mice over 16 wk of age had become weakened, we applied only 500 rads during the irradiation of these mice. The experiments were performed using two *Bach2*-deficient mice. (e) The flow cytometric analysis of the peripheral blood cells to confirm the transplantation. (f) The CT images of the lungs of *Bach2*-deficient mice before and after the transplantation. (g) The histological examination (HE staining) of the lungs 2 mo after the BM transplantation. Bars, 100 µm.

spaces, the surfactant accumulation was greatly reduced (Fig. 10 g). Though we did not measure the function of lungs or saturation level of oxygen in these mice, we judged that they were undoubtedly improved based on the changes in the pathology and CT images. These results showed that the presence of Bach2 in the BM cells prevented the onset of PAP-like disease in *Bach2*-deficient mice and that the BM transplantation was effective for ameliorating PAP even after its onset in this model.

DISCUSSION

Tissue macrophages are not a homogenous population, and it is generally thought that they represent a spectrum of activated phenotypes rather than a discrete stable subpopulation (Mosser and Edwards, 2008). AMs maintain the surfactant homeostasis and play a key regulatory role in pro- and anti-inflammatory responses by acquiring distinct functional phenotypes. However, the factors that regulate the differentiation and function of AMs and the surfactant homeostasis are largely unknown (Lawrence and Natoli, 2011). In this study, we showed that Bach2 was essential for the maintenance of surfactant homeostasis and that this new function of Bach2 involved the regulation of AMs.

Bach2-deficient mice developed the PAP-like accumulation of SPs in the alveolar spaces (Fig. 1). Our results suggest that multiple defects contributed to this phenotype. First, we found that AMs in *Bach2*-deficient mice showed more accumulation of lipids, elevated levels of cholesterol uptake, and faulty handling of PCs compared with WT AMs (Fig. 4, c–e; and Fig. 5). Second, we also observed a reduction in the expression of genes involved in cholesterol metabolism (Fig. 4 e). Lipid homeostasis is regulated by the Pparγ–Abc transporter pathway (Chawla et al., 2001; Ricote et al., 2004), a dysfunction of which results in the formation of foamy AMs (Bates et al., 2005; Thomassen et al., 2007; Baker et al., 2010). Expression of Pparγ and Abcg1 are decreased in the foamy AMs of PAP patients with anti–GM-CSF antibodies and in *GM-CSF*–deficient mice (Thomassen et al., 2007). Because the mRNA levels of *Abca1* and *Abcg1* were both decreased in AMs of *Bach2*-deficient mice (Fig. 4 e), these changes are expected to result in an accumulation of cholesterol, contributing to the generation of foamy AMs observed in *Bach2*-deficient mice

(Fig. 2 a). Because no reduction in Pparγ expression was observed in the absence of Bach2 (Fig. 4 e), Bach2 and Pparγ appear to play distinct roles in the regulation of *Abca1* and *Abcg1*. Third, in addition to the reduced catabolism of surfactants by macrophages, their production appeared to be increased in *Bach2*-deficient mice. *Bach2*-deficient mice showed increased mRNA expression of SP-A and SP-D (Fig. 3 a). This alteration may involve cytokines such as Il-6 that were expressed at higher levels in *Bach2*-deficient AMs (Fig. 7 g). Expression of SP-A and SP-D has been reported to increase in human PAP patients (Kuroki et al., 1998). Enhanced production of SPs may also contribute to the PAP-like phenotype of *Bach2*-deficient mice. Although the exact, more detailed mechanism awaits further investigation, we surmise that the multiple defects, including elevated production of SP as well as impaired handling of protein and lipid components of surfactants, together may place a burden on the surfactant homeostasis in *Bach2*-deficient mice, precipitating PAP over the course of several months after birth (Fig. 1, a and b). Considering the drastic effects of *Bach2* deficiency upon pulmonary surfactant homeostasis, it will be important to examine possible involvement of BACH2 in the etiology of congenital or secondary PAPs in patients. Environmental insults such as trauma, toxin, and infectious agents can perturb the surfactant homeostasis, leading to acute respiratory distress syndrome (Gunasekara et al., 2008; Perez-Gil and Weaver, 2010). Human BACH2 may be involved in such lung diseases as well.

The results presented here and in previous studies suggest a causal link between PAP and M2 polarization of macrophage. The elevated expression of M2-related genes (Fig. 7, c–f; and Fig. 9) showed that AMs and peritoneal macrophages in *Bach2*-deficient mice were skewed in part toward the M2 phenotype. The higher level of *Pparγ1* expression in *Bach2*-deficient AMs (Fig. 4 e) was also consistent with an enhancement of M2 polarization because it is known to promote the M2 phenotype (Odegaard et al., 2007). In contrast, transgenic mice overexpressing Il-4 or Il-13 develop a PAP-like phenotype (Ikegami et al., 2000; Homer et al., 2002), and the Il-4 and Il-13 secreted by T_H2 cells activate macrophages to the M2 phenotype (Gordon, 2003). Although these models of PAP do not necessarily show completely the same pathology of lungs and gene expression patterns in AMs, their features are alike. For example, expression of SP-A and SP-D is selectively up-regulated in the Il-4 transgenic mice (Ikegami et al., 2000; Homer et al., 2002) as in *Bach2*-deficient mice. *SHIP* deficiency leads to M2 polarization, myeloid cell infiltration, and Ym1 crystals in the lung, but the lung pathology appears different from PAP (Rauh et al., 2005). Collectively with these previous studies, our present observations are consistent with the idea that a combination of the excessive M2-like response of AMs and other alterations in *Bach2*-deficient mice contributed to the pathogenesis of the PAP-like disease. Because levels of Il-4 and Il-13 were not increased in the BAL fluid of the *Bach2*-deficient mice (unpublished data), the observed pathology in the lung was not secondary to any change in these cytokine levels.

Although Bach2 is involved in macrophage regulation, it is not clear whether this reflects cell-intrinsic function or not. The altered responses of isolated peritoneal macrophages support the role of Bach2 in macrophages. In addition, we have recently found that the phosphatidylinositol 3-kinase pathway, which is known to promote M2 polarization (Martinez, 2011), inhibits the expression of Bach2 in the peritoneal macrophages (unpublished data). In contrast, we did not observe an elevation in the levels of IL-4 or IL-13 in the lung (unpublished data). These observations support cell-autonomous function of Bach2 in macrophages. Consistent with this interpretation, the expression level of *Irf4* was elevated in *Bach2*-deficient AMs (Fig. 7 f), which is known to promote the M2 phenotype (Cao et al., 2002; Satoh et al., 2010). Thus, we suggest that Bach2 is one of the critical regulators of M1-M2 polarization, limiting the manifestation of a subprogram of M2 phenotype. Because some of the M1-related genes such as *Il6* were expressed at higher levels without Bach2, *Bach2* deficiency did not lead to a simple, general suppression of M1 and activation of M2 genes. It may regulate subprograms for both M1 and M2 phenotypes. However, further studies are required, including cell-specific deletion of *Bach2*, to conclude this interpretation. Identification of direct target genes of Bach2 in macrophages will also be critical.

It remains possible that the altered macrophage phenotype in *Bach2*-deficient mice reflects alterations in both macrophages and microenvironment. This is likely because Bach2 is an important regulator of B cells (Igarashi et al., 2007) and T cells (Roychoudhuri et al., 2013; Tsukumo et al., 2013). It has been reported recently that B1 B cells drive M2 polarization of macrophages in mice (Wong et al., 2010). A recent report suggests a connection between eosinophils and M2-like macrophages (Satoh et al., 2013). Therefore, it is possible that *Bach2*-deficient B cells, T cells, and eosinophils may further contribute to the M2 polarization and the PAP-like disease in the *Bach2*-deficient mice. To further clarify this point, a conditional knockout of *Bach2* in hematopoietic cells will be important.

Based on the observations and discussion above, we propose that *Bach2*-deficient mice provide a valuable mouse model for secondary PAP associated with hematologic disorders. Although an effective treatment for secondary PAP associated with hematological disorders has not been established, there have been reports that secondary PAP was improved by BM transplantation (Cordonnier et al., 1994; Ladeb et al., 1996; Ishii et al., 2011). In this study, even a partial replacement of *Bach2*-deficient BM with WT BM could rescue the accumulation of surfactant in the alveolar spaces (Fig. 10, c and g), showing that BM transplantation is effective for certain types of PAP. The present results also suggest that one should look into the feasibility of identifying therapeutic targets of PAP and other macrophage-related diseases from the downstream target genes or upstream regulators of Bach2.

MATERIALS AND METHODS

Mice. *Bach2*-deficient mice were described previously (Muto et al., 2004). B cell–specific *Blimp-1*–deficient mice (Shapiro-Shelef et al., 2003) were provided by K. Calame (Columbia University, New York, NY). *Bach2*$^{-/-}$*Blimp-1*$^{-/-}$

mice were generated by breeding these mice. CD45.1 congenic mice were purchased from Sankyo Lab Service Corporation, Inc. All experiments involving mice were approved by the Institutional Animal Care and Use Committee of the Tohoku University Environmental & Safety Committee.

Body weight and survival rate curves. WT and *Bach2*-deficient mice were housed under specific pathogen-free conditions. The body weight of the mice was measured every week from 4 until 50 wk of age. Averaged body weight curves were generated for WT mice. Because *Bach2*-deficient mice showed individual variability in body weight and longevity, the data from individual mice were presented separately. The body weight curves and the survival rate curves were generated using Excel (Microsoft) and Delta Graph software (Nihon Poladigital, K.K.) programs, respectively.

Histology and immunohistochemistry. Mice were euthanized using diethyl ether and the lungs were removed, fixed with 4% paraformaldehyde, and embedded in paraffin. Lung sections were stained with hematoxylin and eosin (HE) or PAS stain. Deparaffinized lung sections were incubated with antibodies against SP-A (1:500; Millipore), SP-B (1:500; Millipore), SP-C (1:100; Santa Cruz Biotechnology, Inc.), or SP-D (1:500; Millipore) and visualized by a secondary antibody conjugated with horseradish peroxidase.

BAL fluids and cells. Mice were euthanized using diethyl ether and the trachea was exposed and cannulated. The lungs were flushed two times with 0.8-ml aliquots of PBS. The aliquots were combined and centrifuged at 300 *g* for 5 min to separate the supernatants and BAL cells. The supernatants were stored at −80°C. BAL cells were used for experiments.

Flow cytometry. The collected BAL cells were suspended with staining buffer (PBS with 3% fetal bovine serum) and stained with fluorescent-conjugated antibodies specific for F4/80 (eBioscience) and Gr-1 (BD). The cells were sorted with a FACSAria II (BD). The data were analyzed using FlowJo software (Tree Star).

The collected peritoneal cells were similarly suspended with staining buffer (PBS with 3% fetal bovine serum) and stained with fluorescent-conjugated antibodies specific for F4/80 (eBioscience) and CD11b (BD Biosciences). The cells were sorted with a FACSAria II and data were analyzed with FlowJo software.

Immunofluorescence staining. BAL cells were placed on Matsunami Adhesive silane (MAS)–coated slides and stained with biotin-conjugated anti-CD11c (BD) and anti-Bach2 antiserum (F69-1), or an anti-PU.1 antibody (Santa Cruz Biotechnology, Inc.). Cells were then incubated with streptavidin-conjugated FITC and Alexa Fluor 555–conjugated anti–rabbit IgG antibody. Samples were examined with a confocal laser-scanning microscope (FV-100; Olympus). Photoshop (Adobe) was used for the presentation of images.

Immunoblotting, ELISA, and cytokine antibody array. The BAL fluid was mixed with SDS and heat denaturated. Samples were loaded onto SDS-polyacrylamide gels at 15 µl/well. The immunoblotting analysis was performed with antibodies against SP-A, SP-B, SP-C, or SP-D. The GM-CSF ELISA of BAL fluid was performed using a Mouse GM-CSF ELISA kit (Thermo Fisher Scientific). The cytokine antibody array using the BAL fluid was performed with a RayBio Mouse Cytokine Antibody Array 2 (RayBiotech).

RT-PCR and microarray analysis. The RNA from the lungs and alveolar type 2 epithelial cells was prepared by using the TRIzol reagent (Invitrogen). RNA from the AMs was prepared using an RNeasy Plus Micro kit (QIAGEN). Complementary DNA was synthesized using an Omniscript RT kit (QIAGEN) for RNA from the lungs and a SuperScript First III kit (Invitrogen) for the RNA of AMs. The methods of quantitative PCR and microarray analysis were described previously (Dohi et al., 2008). The analysis of genes was performed using Gene Spring software (Agilent Technologies) and Ingenuity Pathways Analysis software (IPA 9.0; Ingenuity Systems). The primers used are listed in Table S1.

Quantification of internalized NBD-cholesterol. AMs were incubated with RPMI-1640 (2×10^4/100 µl in glass-bottom dishes) and allowed to adhere for 1 h. The cells were added with 1 µM NBD-cholesterol. The dishes were then washed gently with PBS and fixed with 4% paraformaldehyde for 10 min at room temperature. After washing with PBS, fluorescence intensity of the cells with internalized fluorescent cholesterol conjugates was observed upon excitation at 488 nm at a constant intensity in all experiments.

LC-MS/MS analysis. LC-MS/MS was consisted with a NANOSPACE SI-2 HPLC system (Shiseido) and a TSQ Quantum Ultra (Thermo Fisher Scientific) triple quadrupole mass spectrometer equipped with a heated ESI source. Samples were analyzed by precursor ion scanning mode in a range of *m/z* 520 to 1,000 in positive ionization mode via collision induced dissociation (CID). After fragmentation of CID gas with 31 eV of collision energy, PC molecules produced a fragment with *m/z* 184 corresponding to the protonated phosphocoline head group according to a previous study (Brügger et al., 1997). The optimum value of the MS parameters for spray voltage, sheath gas pressure, axillary gas pressure, vaporizer temperature, capillary temperature, and collision pressure were set at 3.0 kV, 35 psi, 20 psi, 350°C, 270°C, and 0.7 mTorr, respectively. Liquid chromatographic separation was performed using a Capcell Pak Silica SG120 (150 mm × 2 mm i.d., 5-µm particle size; Shiseido) column with a hydrophilic interaction chromatography elution. The mobile phases were 5 mmol/liter ammonium formate (A) and acetonitrile (B). The gradient program was as follows: initial elution with 100% B followed by a linear gradient to 82.5% B from 0 to 15 min, and immediately decreased 30% B at 17 min. Then, we returned to the initial conditions for 2 min until the end of the run. The total run time was 20 min. The mobile phase flow rate was 400 µl/min. Column effluent was introduced into the MS between 3.0 and 22.5 min after injection.

Sample preparation for LC-MS/MS was done according to a previous study (Saigusa et al., 2012). An automated cell counter was used to calculate cell numbers and 25,000 cells were used for the sample preparation. 100 µl methanol was added into the sample of AMs. Because cell debris may be counted, we may have overestimated the numbers of the cells. The resulting mixture was homogenized for 5 min in an ultrasonic bath. After centrifugation at 16,400 *g* for 10 min, the supernatant was transferred into a new 2.0-ml siliconized plastic tube. Then, an internal standard (IS; PC14:0/14:0, 1 µmol/liter, 50 µl) was added, and the mixture was homogenized for 5 min in an ultrasonic bath and centrifuged at 16,400 *g* for 10 min. Then, the supernatant was transferred into a new siliconized plastic tube and passed through a filter (pore size: 0.2 µm; YMC). Subsequently, 5 µl of the filtered solution was injected into the LC-MS/MS system. The values of composition were calculated by the ratio of IS, and comparisons between WT and KO groups were made using Student's independent *t* test. The representative spices of PCs in lung macrophages were extracted according to a previous study (Postle et al., 2006) and assigned with the Lipid Search (Mitsui Knowledge Industry) software using additional independent high-resolution data by a Q Exactive (Thermo Fisher Scientific).

Isolation of alveolar type 2 epithelial cells. Alveolar type 2 epithelial cells were isolated as described previously (Corti et al., 1996) with some modifications. Anti-CD32 antibody was omitted for the purification.

Peritoneal macrophages and BMDMs. Peritoneal macrophages and BMDMs were isolated from WT or *Bach2*-deficient mice, as previously described (Fleetwood et al., 2007; Satoh et al., 2010), and were cultured in RPMI-1640 medium containing 10% (vol/vol) fetal bovine serum and 10 ng/ml GM-CSF. 10 µg/ml LPS (InvivoGen) and 20 ng/ml IL-4 (Sigma-Aldrich) were added as M1 and M2 macrophage inducer, respectively.

Intracellular staining. IL-4–stimulated cells were washed in staining buffer, PBS containing BSA (0.5%), and sodium azide (0.05%) and blocked with

Mouse Fc block antibody (BD). The cells were first fixed by incubation with 1% paraformaldehyde at room temperature for 10 min, and then permeabilized in staining buffer containing 0.03% saponin (Sigma-Aldrich). Staining buffer containing 0.3% saponin was used to stain the cells with 20 µl PE-labeled antibody specific to phospho-STAT6 (BD) or PE-labeled mouse IgG1κ isotype control (BD) for 30 min. After washing with 0.03% saponin buffer, cells were analyzed by flow cytometry on the FACSAria II. Data were analyzed using FlowJo software.

Responses to cytokines. Human H441 cells were seeded in 6-well plates at 2.5×10^5 per well. The cells were incubated for 1 or 2 d in the presence or absence of indicated human cytokines at 100 ng/ml. Whole cell extracts were analyzed by immunoblotting using anti–SP-A antibody.

BM transplantation. The 8-wk-old *Bach2*-deficient mice were subjected to lethal γ-irradiation in two doses of 500 rads each (for a total of 1,000 rads) 3 h apart, and were injected with either WT or *Bach2*-deficient BM (2×10^6 cells in 150 µl PBS) via a tail vein.The *Bach2*-deficient mice >16 wk of age were subjected to sublethal γ-irradiation of a single dose of 500 rads, and were injected with WT BM as above. After the BM transplantation, mice were fed antibiotics in their drinking water (30 mg/ml ampicillin). Bottles of water containing antibiotics were exchanged every 2–3 d, and the administration of the antibiotic was maintained for 4 wk. Because AMs are repopulated by donor cells 60 d after BM transplantation (Matute-Bello et al., 2004; Satoh et al., 2010), the mice were euthanized and the lungs were assessed histologically 2 mo after the BM transplant. Peripheral blood cells were depleted of RBCs and stained with fluorescent-conjugated antibodies specific for CD45.1 and CD45.2 (BD).

Chest computed-tomography (CT). The mice were anesthetized by an intraperitoneal injection of tribromoethanol (Sigma-Aldrich). CT images of the lungs were taken with a Latheta LCT-200 (Hitachi Aloka Medical).

Statistical analysis. The data are presented as the means + SD. All of the statistical analyses were done using two-tailed Student's *t*-tests.

Online supplemental material. Primers used in this study are listed in Table S1. Results of GO analysis are in Tables S2 and S3. Online supplemental material is available at http://www.jem.org/cgi/content/full/jem.20130028/DC1.

We thank Dr. Hiroshi Kubo (Tohoku University) for valuable advice and instructing us in the technique used for the isolation of type 2 epithelial cells, Dr. Takuji Suzuki (Cincinnati Children's Hospital Medical Center) for valuable advice on PAP, and Dr. Masao Ono (Tohoku University) for valuable advice on pathological analysis. The interpretation of the data was enriched by discussions with Dr. Kazushige Ota and other members of our laboratories. We are indebted to Drs. Rahul Roychoudhuri and Nicholas P. Restifo (National Institutes of Health) for discussion and comments on the manuscript.

Part of this study was supported by Biomedical Research Core of Tohoku University School of Medicine. This work was supported by Grants-in-aid and the Network Medicine Global-COE Program from the Ministry of Education, Culture, Sports, Science and Technology, Japan. Additional initiative support was from Takeda Foundation. Restoration of laboratory damages from 2011 Tohoku earthquake was supported in part by the Astellas Foundation for Research on Metabolic Disorders, Banyu Foundation, Naito Foundation, A. Miyazaki, and A. Iida.

The authors have no conflicting financial interests.

Submitted: 5 January 2013
Accepted: 10 September 2013

REFERENCES

Ando, J., K. Tamayose, K. Sugimoto, and K. Oshimi. 2002. Late appearance of t(1;19)(q11;q11) in myelodysplastic syndrome associated with dysplastic eosinophilia and pulmonary alveolar proteinosis. *Cancer Genet. Cytogenet.* 139:14–17. http://dx.doi.org/10.1016/S0165-4608(02)00652-0

Baker, A.D., A. Malur, B.P. Barna, S. Ghosh, M.S. Kavuru, A.G. Malur, and M.J. Thomassen. 2010. Targeted PPARgamma deficiency in alveolar macrophages disrupts surfactant catabolism. *J. Lipid Res.* 51:1325–1331. http://dx.doi.org/10.1194/jlr.M001651

Bates, S.R., J.Q. Tao, H.L. Collins, O.L. Francone, and G.H. Rothblat. 2005. Pulmonary abnormalities due to ABCA1 deficiency in mice. *Am. J. Physiol. Lung Cell. Mol. Physiol.* 289:L980–L989. http://dx.doi.org/10.1152/ajplung.00234.2005

Blanchard, P.G., W.T. Festuccia, V.P. Houde, P. St-Pierre, S. Brûlé, V. Turcotte, M. Côté, K. Bellmann, A. Marette, and Y. Deshaies. 2012. Major involvement of mTOR in the PPARγ-induced stimulation of adipose tissue lipid uptake and fat accretion. *J. Lipid Res.* 53:1117–1125. http://dx.doi.org/10.1194/jlr.M021485

Bonfield, T.L., C.F. Farver, B.P. Barna, A. Malur, S. Abraham, B. Raychaudhuri, M.S. Kavuru, and M.J. Thomassen. 2003. Peroxisome proliferator-activated receptor-gamma is deficient in alveolar macrophages from patients with alveolar proteinosis. *Am. J. Respir. Cell Mol. Biol.* 29:677–682. http://dx.doi.org/10.1165/rcmb.2003-0148OC

Borie, R., C. Danel, M.P. Debray, C. Taille, M.C. Dombret, M. Aubier, R. Epaud, and B. Crestani. 2011. Pulmonary alveolar proteinosis. *Eur Respir Rev.* 20:98–107. http://dx.doi.org/10.1183/09059180.00001311

Brügger, B., G. Erben, R. Sandhoff, F.T. Wieland, and W.D. Lehmann. 1997. Quantitative analysis of biological membrane lipids at the low picomole level by nano-electrospray ionization tandem mass spectrometry. *Proc. Natl. Acad. Sci. USA.* 94:2339–2344. http://dx.doi.org/10.1073/pnas.94.6.2339

Buechner, H.A., and A. Ansari. 1969. Acute silico-proteinosis. A new pathologic variant of acute silicosis in sandblasters, characterized by histologic features resembling alveolar proteinosis. *Dis. Chest.* 55:274–278. http://dx.doi.org/10.1378/chest.55.4.274

Cao, S., J. Liu, M. Chesi, P.L. Bergsagel, I.C. Ho, R.P. Donnelly, and X. Ma. 2002. Differential regulation of IL-12 and IL-10 gene expression in macrophages by the basic leucine zipper transcription factor c-Maf fibrosarcoma. *J. Immunol.* 169:5715–5725.

Chawla, A., W.A. Boisvert, C.H. Lee, B.A. Laffitte, Y. Barak, S.B. Joseph, D. Liao, L. Nagy, P.A. Edwards, L.K. Curtiss, et al. 2001. A PPAR gamma-LXR-ABCA1 pathway in macrophages is involved in cholesterol efflux and atherogenesis. *Mol. Cell.* 7:161–171. http://dx.doi.org/10.1016/S1097-2765(01)00164-2

Cordonnier, C., J. Fleury-Feith, E. Escudier, K. Atassi, and J.F. Bernaudin. 1994. Secondary alveolar proteinosis is a reversible cause of respiratory failure in leukemic patients. *Am. J. Respir. Crit. Care Med.* 149:788–794. http://dx.doi.org/10.1164/ajrccm.149.3.8118651

Corti, M., A.R. Brody, and J.H. Harrison. 1996. Isolation and primary culture of murine alveolar type II cells. *Am. J. Respir. Cell Mol. Biol.* 14:309–315. http://dx.doi.org/10.1165/ajrcmb.14.4.8600933

Dirksen, U., R. Nishinakamura, P. Groneck, U. Hattenhorst, L. Nogee, R. Murray, and S. Burdach. 1997. Human pulmonary alveolar proteinosis associated with a defect in GM-CSF/IL-3/IL-5 receptor common beta chain expression. *J. Clin. Invest.* 100:2211–2217. http://dx.doi.org/10.1172/JCI119758

Dohi, Y., T. Ikura, Y. Hoshikawa, Y. Katoh, K. Ota, A. Nakanome, A. Muto, S. Omura, T. Ohta, A. Ito, et al. 2008. Bach1 inhibits oxidative stress-induced cellular senescence by impeding p53 function on chromatin. *Nat. Struct. Mol. Biol.* 15:1246–1254. http://dx.doi.org/10.1038/nsmb.1516

Dranoff, G., A.D. Crawford, M. Sadelain, B. Ream, A. Rashid, R.T. Bronson, G.R. Dickersin, C.J. Bachurski, E.L. Mark, J.A. Whitsett, et al. 1994. Involvement of granulocyte-macrophage colony-stimulating factor in pulmonary homeostasis. *Science.* 264:713–716. http://dx.doi.org/10.1126/science.8171324

Fleetwood, A.J., T. Lawrence, J.A. Hamilton, and A.D. Cook. 2007. Granulocyte-macrophage colony-stimulating factor (CSF) and macrophage CSF-dependent macrophage phenotypes display differences in cytokine profiles and transcription factor activities: implications for CSF blockade in inflammation. *J. Immunol.* 178:5245–5252.

Gordon, S. 2003. Alternative activation of macrophages. *Nat. Rev. Immunol.* 3:23–35. http://dx.doi.org/10.1038/nri978

Gunasekara, L., W.M. Schoel, S. Schürch, and M.W. Amrein. 2008. A comparative study of mechanisms of surfactant inhibition. *Biochim. Biophys. Acta.* 1778:433–444. http://dx.doi.org/10.1016/j.bbamem.2007.10.027

Harris, J.O. 1979. Pulmonary alveolar proteinosis: abnormal in vitro function of alveolar macrophages. *Chest*. 76:156–159. http://dx.doi.org/10.1378/chest.76.2.156

Homer, R.J., T. Zheng, G. Chupp, S. He, Z. Zhu, Q. Chen, B. Ma, R.D. Hite, L.I. Gobran, S.A. Rooney, and J.A. Elias. 2002. Pulmonary type II cell hypertrophy and pulmonary lipoproteinosis are features of chronic IL-13 exposure. *Am. J. Physiol. Lung Cell. Mol. Physiol.* 283:L52–L59.

Igarashi, K., K. Ochiai, and A. Muto. 2007. Architecture and dynamics of the transcription factor network that regulates B-to-plasma cell differentiation. *J. Biochem.* 141:783–789. http://dx.doi.org/10.1093/jb/mvm106

Ikegami, M., J.A. Whitsett, Z.C. Chroneos, G.F. Ross, J.A. Reed, C.J. Bachurski, and A.H. Jobe. 2000. IL-4 increases surfactant and regulates metabolism in vivo. *Am. J. Physiol. Lung Cell. Mol. Physiol.* 278:L75–L80.

Inoue, Y., B.C. Trapnell, R. Tazawa, T. Arai, T. Takada, N. Hizawa, Y. Kasahara, K. Tatsumi, M. Hojo, T. Ichiwata, et al; Japanese Center of the Rare Lung Diseases Consortium. 2008. Characteristics of a large cohort of patients with autoimmune pulmonary alveolar proteinosis in Japan. *Am. J. Respir. Crit. Care Med.* 177:752–762. http://dx.doi.org/10.1164/rccm.200708-1271OC

Ishii, H., R. Tazawa, C. Kaneko, T. Saraya, Y. Inoue, E. Hamano, Y. Kogure, K. Tomii, M. Terada, T. Takada, et al. 2011. Clinical features of secondary pulmonary alveolar proteinosis: pre-mortem cases in Japan. *Eur. Respir. J.* 37:465–468. http://dx.doi.org/10.1183/09031936.00092910

Iyonaga, K., M. Suga, T. Yamamoto, H. Ichiyasu, H. Miyakawa, and M. Ando. 1999. Elevated bronchoalveolar concentrations of MCP-1 in patients with pulmonary alveolar proteinosis. *Eur. Respir. J.* 14:383–389. http://dx.doi.org/10.1034/j.1399-3003.1999.14b24.x

Kang, K., S.M. Reilly, V. Karabacak, M.R. Gangl, K. Fitzgerald, B. Hatano, and C.H. Lee. 2008. Adipocyte-derived Th2 cytokines and myeloid PPARdelta regulate macrophage polarization and insulin sensitivity. *Cell Metab.* 7:485–495. http://dx.doi.org/10.1016/j.cmet.2008.04.002

Keller, C.A., A. Frost, P.T. Cagle, and J.L. Abraham. 1995. Pulmonary alveolar proteinosis in a painter with elevated pulmonary concentrations of titanium. *Chest.* 108:277–280. http://dx.doi.org/10.1378/chest.108.1.277

Kitamura, T., N. Tanaka, J. Watanabe, S. Uchida, S. Kanegasaki, Y. Yamada, and K. Nakata. 1999. Idiopathic pulmonary alveolar proteinosis as an autoimmune disease with neutralizing antibody against granulocyte/macrophage colony-stimulating factor. *J. Exp. Med.* 190:875–880. http://dx.doi.org/10.1084/jem.190.6.875

Kohyama, M., W. Ise, B.T. Edelson, P.R. Wilker, K. Hildner, C. Mejia, W.A. Frazier, T.L. Murphy, and K.M. Murphy. 2009. Role for Spi-C in the development of red pulp macrophages and splenic iron homeostasis. *Nature.* 457:318–321. http://dx.doi.org/10.1038/nature07472

Kuroki, Y., H. Takahashi, H. Chiba, and T. Akino. 1998. Surfactant proteins A and D: disease markers. *Biochim. Biophys. Acta.* 1408:334–345. http://dx.doi.org/10.1016/S0925-4439(98)00079-9

Ladeb, S., J. Fleury-Feith, E. Escudier, J. Tran Van Nhieu, J.F. Bernaudin, and C. Cordonnier. 1996. Secondary alveolar proteinosis in cancer patients. *Support. Care Cancer.* 4:420–426. http://dx.doi.org/10.1007/BF01880639

Lawrence, T., and G. Natoli. 2011. Transcriptional regulation of macrophage polarization: enabling diversity with identity. *Nat. Rev. Immunol.* 11:750–761. http://dx.doi.org/10.1038/nri3088

Martinez, F.O. 2011. Regulators of macrophage activation. *Eur. J. Immunol.* 41:1531–1534. http://dx.doi.org/10.1002/eji.201141670

Matute-Bello, G., J.S. Lee, C.W. Frevert, W.C. Liles, S. Sutlief, K. Ballman, V. Wong, A. Selk, and T.R. Martin. 2004. Optimal timing to repopulation of resident alveolar macrophages with donor cells following total body irradiation and bone marrow transplantation in mice. *J. Immunol. Methods.* 292:25–34. http://dx.doi.org/10.1016/j.jim.2004.05.010

Mosser, D.M., and J.P. Edwards. 2008. Exploring the full spectrum of macrophage activation. *Nat. Rev. Immunol.* 8:958–969. http://dx.doi.org/10.1038/nri2448

Muto, A., H. Hoshino, L. Madisen, N. Yanai, M. Obinata, H. Karasuyama, N. Hayashi, H. Nakauchi, M. Yamamoto, M. Groudine, and K. Igarashi. 1998. Identification of Bach2 as a B-cell-specific partner for small maf proteins that negatively regulate the immunoglobulin heavy chain gene 3′ enhancer. *EMBO J.* 17:5734–5743. http://dx.doi.org/10.1093/emboj/17.19.5734

Muto, A., S. Tashiro, O. Nakajima, H. Hoshino, S. Takahashi, E. Sakoda, D. Ikebe, M. Yamamoto, and K. Igarashi. 2004. The transcriptional programme of antibody class switching involves the repressor Bach2. *Nature.* 429:566–571. http://dx.doi.org/10.1038/nature02596

Muto, A., K. Ochiai, Y. Kimura, A. Itoh-Nakadai, K.L. Calame, D. Ikebe, S. Tashiro, and K. Igarashi. 2010. Bach2 represses plasma cell gene regulatory network in B cells to promote antibody class switch. *EMBO J.* 29:4048–4061. http://dx.doi.org/10.1038/emboj.2010.257

Nelson, S.M., X. Lei, and K.S. Prabhu. 2011. Selenium levels affect the IL-4-induced expression of alternative activation markers in murine macrophages. *J. Nutr.* 141:1754–1761. http://dx.doi.org/10.3945/jn.111.141176

Nogee, L.M., D.E. de Mello, L.P. Dehner, and H.R. Colten. 1993. Brief report: deficiency of pulmonary surfactant protein B in congenital alveolar proteinosis. *N. Engl. J. Med.* 328:406–410. http://dx.doi.org/10.1056/NEJM199302113280606

Nogee, L.M., A.E. Dunbar III, S.E. Wert, F. Askin, A. Hamvas, and J.A. Whitsett. 2001. A mutation in the surfactant protein C gene associated with familial interstitial lung disease. *N. Engl. J. Med.* 344:573–579. http://dx.doi.org/10.1056/NEJM200102223440805

Ochiai, K., Y. Katoh, T. Ikura, Y. Hoshikawa, T. Noda, H. Karasuyama, S. Tashiro, A. Muto, and K. Igarashi. 2006. Plasmacytic transcription factor Blimp-1 is repressed by Bach2 in B cells. *J. Biol. Chem.* 281:38226–38234. http://dx.doi.org/10.1074/jbc.M607592200

Odegaard, J.I., R.R. Ricardo-Gonzalez, M.H. Goforth, C.R. Morel, V. Subramanian, L. Mukundan, A. Red Eagle, D. Vats, F. Brombacher, A.W. Ferrante, and A. Chawla. 2007. Macrophage-specific PPARgamma controls alternative activation and improves insulin resistance. *Nature.* 447:1116–1120. http://dx.doi.org/10.1038/nature05894

Oyake, T., K. Itoh, H. Motohashi, N. Hayashi, H. Hoshino, M. Nishizawa, M. Yamamoto, and K. Igarashi. 1996. Bach proteins belong to a novel family of BTB-basic leucine zipper transcription factors that interact with MafK and regulate transcription through the NF-E2 site. *Mol. Cell. Biol.* 16:6083–6095.

Paine, R. III, S.B. Morris, H. Jin, S.E. Wilcoxen, S.M. Phare, B.B. Moore, M.J. Coffey, and G.B. Toews. 2001. Impaired functional activity of alveolar macrophages from GM-CSF-deficient mice. *Am. J. Physiol. Lung Cell. Mol. Physiol.* 281:L1210–L1218.

Perez-Gil, J., and T.E. Weaver. 2010. Pulmonary surfactant pathophysiology: current models and open questions. *Physiology* (*Bethesda*). 25:132–141. http://dx.doi.org/10.1152/physiol.00006.2010

Postle, A.D., L.W. Gonzales, W. Bernhard, G.T. Clark, M.H. Godinez, R.I. Godinez, and P.L. Ballard. 2006. Lipidomics of cellular and secreted phospholipids from differentiated human fetal type II alveolar epithelial cells. *J. Lipid Res.* 47:1322–1331. http://dx.doi.org/10.1194/jlr.M600054-JLR200

Rauh, M.J., V. Ho, C. Pereira, A. Sham, L.M. Sly, V. Lam, L. Huxham, A.I. Minchinton, A. Mui, and G. Krystal. 2005. SHIP represses the generation of alternatively activated macrophages. *Immunity.* 23:361–374. http://dx.doi.org/10.1016/j.immuni.2005.09.003

Ricote, M., A.F. Valledor, and C.K. Glass. 2004. Decoding transcriptional programs regulated by PPARs and LXRs in the macrophage: effects on lipid homeostasis, inflammation, and atherosclerosis. *Arterioscler. Thromb. Vasc. Biol.* 24:230–239. http://dx.doi.org/10.1161/01.ATV.0000103951.67680.B1

Roychoudhuri, R., K. Hirahara, K. Mousavi, D. Clever, C.A. Klebanoff, M. Bonelli, G. Sciumè, H. Zare, G. Vahedi, B. Dema, et al. 2013. BACH2 represses effector programs to stabilize T(reg)-mediated immune homeostasis. *Nature.* 498:506–510. http://dx.doi.org/10.1038/nature12199

Ruben, F.L., and T.S. Talamo. 1986. Secondary pulmonary alveolar proteinosis occurring in two patients with acquired immune deficiency syndrome. *Am. J. Med.* 80:1187–1190. http://dx.doi.org/10.1016/0002-9343(86)90683-2

Saigusa, D., K. Shiba, A. Inoue, K. Hama, M. Okutani, N. Iida, M. Saito, K. Suzuki, T. Kaneko, N. Suzuki, et al. 2012. Simultaneous quantitation of sphingoid bases and their phosphates in biological samples by liquid chromatography/electrospray ionization tandem mass spectrometry. *Anal. Bioanal. Chem.* 403:1897–1905. http://dx.doi.org/10.1007/s00216-012-6004-9

Satoh, T., O. Takeuchi, A. Vandenbon, K. Yasuda, Y. Tanaka, Y. Kumagai, T. Miyake, K. Matsushita, T. Okazaki, T. Saitoh, et al. 2010. The Jmjd3-Irf4 axis regulates M2 macrophage polarization and host responses against helminth infection. *Nat. Immunol.* 11:936–944. http://dx.doi.org/10.1038/ni.1920

Satoh, T., H. Kidoya, H. Naito, M. Yamamoto, N. Takemura, K. Nakagawa, Y. Yoshioka, E. Morii, N. Takakura, O. Takeuchi, and S. Akira. 2013. Critical role of Trib1 in differentiation of tissue-resident M2-like macrophages. *Nature.* 495:524–528. http://dx.doi.org/10.1038/nature11930

Sciammas, R., A.L. Shaffer, J.H. Schatz, H. Zhao, L.M. Staudt, and H. Singh. 2006. Graded expression of interferon regulatory factor-4 coordinates isotype switching with plasma cell differentiation. *Immunity.* 25:225–236. http://dx.doi.org/10.1016/j.immuni.2006.07.009

Shapiro-Shelef, M., K.I. Lin, L.J. McHeyzer-Williams, J. Liao, M.G. McHeyzer-Williams, and K. Calame. 2003. Blimp-1 is required for the formation of immunoglobulin secreting plasma cells and pre-plasma memory B cells. *Immunity.* 19:607–620. http://dx.doi.org/10.1016/S1074-7613(03)00267-X

Shibata, Y., P.Y. Berclaz, Z.C. Chroneos, M. Yoshida, J.A. Whitsett, and B.C. Trapnell. 2001. GM-CSF regulates alveolar macrophage differentiation and innate immunity in the lung through PU.1. *Immunity.* 15:557–567. http://dx.doi.org/10.1016/S1074-7613(01)00218-7

Takeda, K., T. Tanaka, W. Shi, M. Matsumoto, M. Minami, S. Kashiwamura, K. Nakanishi, N. Yoshida, T. Kishimoto, and S. Akira. 1996. Essential role of Stat6 in IL-4 signalling. *Nature.* 380:627–630. http://dx.doi.org/10.1038/380627a0

Thomassen, M.J., B.P. Barna, A.G. Malur, T.L. Bonfield, C.F. Farver, A. Malur, H. Dalrymple, M.S. Kavuru, and M. Febbraio. 2007. ABCG1 is deficient in alveolar macrophages of GM-CSF knockout mice and patients with pulmonary alveolar proteinosis. *J. Lipid Res.* 48:2762–2768. http://dx.doi.org/10.1194/jlr.P700022-JLR200

Trapnell, B.C., J.A. Whitsett, and K. Nakata. 2003. Pulmonary alveolar proteinosis. *N. Engl. J. Med.* 349:2527–2539. http://dx.doi.org/10.1056/NEJMra023226

Trapnell, B.C., B.C. Carey, K. Uchida, and T. Suzuki. 2009. Pulmonary alveolar proteinosis, a primary immunodeficiency of impaired GM-CSF stimulation of macrophages. *Curr. Opin. Immunol.* 21:514–521. http://dx.doi.org/10.1016/j.coi.2009.09.004

Tsukumo, S., M. Unno, A. Muto, A. Takeuchi, K. Kometani, T. Kurosaki, K. Igarashi, and T. Saito. 2013. Bach2 maintains T cells in a naive state by suppressing effector memory-related genes. *Proc. Natl. Acad. Sci. USA.* 110:10735–10740. http://dx.doi.org/10.1073/pnas.1306691110

Wong, S.C., A.L. Puaux, M. Chittezhath, I. Shalova, T.S. Kajiji, X. Wang, J.P. Abastado, K.P. Lam, and S.K. Biswas. 2010. Macrophage polarization to a unique phenotype driven by B cells. *Eur. J. Immunol.* 40:2296–2307. http://dx.doi.org/10.1002/eji.200940288

Yoshida, M., M. Ikegami, J.A. Reed, Z.C. Chroneos, and J.A. Whitsett. 2001. GM-CSF regulates protein and lipid catabolism by alveolar macrophages. *Am. J. Physiol. Lung Cell. Mol. Physiol.* 280:L379–L386.